



# ALGORITHM THEORETICAL BASIS DOCUMENT

## GOME-2 tropospheric BrO data-records

Prepared  
by: Klaus-Peter Heue DLR  
Nan Hao formerly DLR  
Nicolas Theys BIRA  
Pieter Valks DLR

## Signatures

<b>Action: Name</b>	<b>Affiliation</b>	<b>Function</b>	<b>Date</b>	<b>Sign.</b>
prepared by: K.-P. Heue N. Theys N. Hao P. Valks	DLR-MF BIRA formerly DLR DLR-MF	AC SAF Project Scientist AC SAF Project Scientist AC SAF project Scientist AC SAF Project Manager	10.12.2020	
released by: P. Valks	DLR-MF	AC SAF Project Manager	18.12.2020	

## Distribution List

<b>Function</b>	<b>Organization</b>
GOME-2 / AC SAF Team	DLR-MF, DLR-DFD
AC SAF Team	EUMETSAT, FMI, KNMI, DMI, BIRA, AUTH, various

## Document Change Log

<b>Issue</b>	<b>Rev.</b>	<b>Date</b>	<b>Section</b>	<b>Description of Change</b>
1	A	9 June 2016	All	Completely new
1	B	10 Dec 2020	All	Change SAF naming to AC SAF Updates for DRR
1	C	7 Dec 2021	2	algorithm updates solar reference, updated AMF calculation

## Table of Contents

<b>TABLE OF CONTENTS</b> .....	<b>3</b>
<b>EUMETSAT SATELLITE APPLICATION FACILITY ON ATMOSPHERIC COMPOSITION MONITORING (AC SAF)</b> .....	<b>4</b>
Background.....	4
Objective .....	4
Product categories, timeliness and dissemination .....	4
<b>1. INTRODUCTION</b> .....	<b>6</b>
1.1 Purpose and scope .....	6
1.2 MetOp and GOME-2 .....	6
<b>2. THE BRO COLUMN ALGORITHM</b> .....	<b>7</b>
2.1 DOAS slant column fitting .....	7
2.2 Equatorial offset correction.....	8
2.3 AMF and VCD determination .....	8
2.4 Tropospheric BrO column .....	9
2.4.1 Stratospheric BrO correction .....	9
2.5 Tropospheric Air Mass Factor and VCD computation.....	9
<b>3. REFERENCES</b> .....	<b>11</b>

---

## EUMETSAT SATELLITE APPLICATION FACILITY ON ATMOSPHERIC COMPOSITION MONITORING (AC SAF)

### Background

The need for atmospheric chemistry monitoring was first realized when severe loss of stratospheric ozone was detected over the Polar Regions. At the same time, increased levels of ultraviolet radiation were observed.

Ultraviolet radiation is known to be dangerous to humans and animals (causing e.g. skin cancer, cataract, immune suppression) and having harmful effects on agriculture, forests and oceanic food chain. In addition, the global warming - besides affecting the atmospheric chemistry - also enhances the ozone depletion by cooling the stratosphere. Combined, these phenomena have immense effects on the whole planet. Therefore, monitoring the chemical composition of the atmosphere is a very important duty for EUMETSAT and the world-wide scientific community.

### Objective

The main objectives of the AC SAF is to process, archive, validate and disseminate atmospheric composition products ( $O_3$ ,  $NO_2$ ,  $SO_2$ , BrO, HCHO,  $H_2O$  and OCIO), aerosol products and surface ultraviolet radiation products utilising the satellites of EUMETSAT. The majority of the AC SAF products are based on data from the GOME-2 spectrometers onboard MetOp-A, MetOp-B and MetOp-C satellites.

Another important task of the AC SAF is the research and development in radiative transfer modelling and inversion methods for obtaining long-term, high-quality atmospheric composition products from the satellite measurements.

### Product categories, timeliness and dissemination

Data products are divided in two categories depending on how quickly they are available to users:

*Near real-time products* are available in less than three hours after measurement. These products are disseminated via EUMETCast, WMO GTS or internet.

- Near real-time trace gas columns
  - $O_3$ ,  $NO_2$ , HCHO,  $SO_2$
- Near real-time ozone profiles
  - coarse and high-resolution
- Near real-time absorbing aerosol indexes
  - from main science channels and polarization measurement detectors
- Near real-time UV indexes
  - clear-sky and cloud-corrected

*Offline products* are available in two weeks after measurement and disseminated via dedicated web services at EUMETSAT, FMI and DLR.

- Offline trace gas columns
  - $O_3$ ,  $NO_2$ ,  $SO_2$ , BrO, HCHO,  $H_2O$  and OCIO
- Offline ozone profiles
  - coarse and high-resolution
- Offline absorbing aerosol indexes
  - from main science channels and polarization measurement detectors
- Offline surface UV

*Data record products* are available for a fixed time range (e.g. 1.1.2007 to 30.6.2020). In contrast to the NRTI and OFFL products, the datasets are not automatically continued based on new observations. The respective data-sets are provided via dedicated web services at EUMETSAT, FMI and DLR.

Available data records are:

- GOME-2 tropospheric BrO columns
- GOME-2 glyoxal columns
- GOME-2 monthly gridded (Level-3) NO<sub>2</sub> and H<sub>2</sub>O columns

**More information about the AC SAF project, products and services:**

<http://acsaf.org/>

**AC SAF Helpdesk:** helpdesk@acsaf.org

## 1. INTRODUCTION

### 1.1 Purpose and scope

This document describes the operational algorithm for the retrieval of tropospheric bromine monoxide (BrO) columns from the GOME-2 instruments, as part of the AC-SAF. This algorithm has been used to generate tropospheric BrO data records from GOME-2/MetOp-A (period: January 2007- December 2017) and GOME-2/MetOp-B (period: December 2012- June 2020).

The product format is described in the corresponding Product User Manual (Heue et al., 2020).

In this document, the terms GOME/ERS-2, GOME-2/MetOp-A and GOME-2/MetOp-B are used to reference the specific instruments. The term GOME-2 applies to both GOME-2 instruments on MetOp-A and -B.

### 1.2 MetOp and GOME-2

The instruments on the MetOp satellites produce high-resolution images of the Earth's surface, vertical temperature and humidity profiles, and temperatures of the land and ocean surface on a global basis. In addition, there are instruments for monitoring ozone and other key trace gases in the troposphere and stratosphere, and for measuring the wind flow over the oceans.

MetOp-A was launched on 19 October 2006 as part of the Initial Joint Polar System (IJPS) in cooperation with NOAA in the USA. The second polar-orbiting satellite in the series, MetOp-B, was successfully launched on 17 September 2012. MetOp-A and MetOp-B are flying on sun-synchronous orbits with a repeat cycle of 29 days and an Equator crossing time of 09:30 local time (descending mode). GOME-2 extends the long-term atmospheric composition measurements started by the ESA (European Space Agency) missions GOME/ERS-2 (European Remote Sensing Satellite; 1995) and continued with SCIAMACHY (SCanning Imaging Absorption spectrometer for Atmospheric CHartographY)/ENVISAT (2002).

GOME-2 is a nadir-scanning UV-VIS spectrometer (Munro et al., 2006), covering the spectral range between 240 and 790 nm with a spectral resolution between 0.26 nm and 0.51 nm (FWHM). Additionally, two polarisation components are measured with polarisation measurement devices (PMDs) at 30 broad-band channels covering the full spectral range. The default swath width of the GOME-2 scan is 1920 km, which enables global coverage in about 1.5 days. GOME-2 ground pixels have a default footprint size of 80x40 km<sup>2</sup> in the forward scan, which is four times smaller than those for GOME (320x40 km<sup>2</sup>), but larger than those for SCIAMACHY (30x60 km<sup>2</sup>) and OMI (24x13 km<sup>2</sup> at nadir). Owing to a non-linear movement of the scan mirror, the ground pixel size remains nearly constant over the full scan. In the tandem mode, GOME-2/Metop-A operates on a reduced swath width of 960 km with an increased spatial resolution (approx. 40x40 km<sup>2</sup>), while GOME-2/Metop-B operates on a nominal wide swath at 1920 km. This implementation increases both the daily coverage and the spatial resolution of GOME-2 measurements. GOME-2 tandem operations started on 15 July 2013.

Based on the successful work with the GOME data processors, the German Aerospace Centre (DLR) plays a major role in the design, implementation and operation of the GOME-2 ground segment for the trace gas column products. DLR is a partner in the Satellite Application Facility on Ozone and Atmospheric Chemistry Monitoring (ACSAF), which is part of the EUMETSAT Polar System (EPS) ground segment, and is responsible in this project for the generation of total column amounts of the various trace gases and cloud properties which may be retrieved from GOME-2 level 1b products.

## 2. THE BRO COLUMN ALGORITHM

### 2.1 DOAS slant column fitting

The DOAS algorithm for BrO is based on the DOAS algorithm for total ozone as described in details in Sect. 2.2 of the ATBD (Valks et al., 2019) for the operational GOME-2 trace gas column products. The original GOME algorithm used the 344.7-359 nm wavelength range for the DOAS slant column fit of BrO (so-called “GOME” fitting-window) (Richter et al., 1998). As a result of the smaller pixel size of GOME-2 observations (40x80 / 40x40 km<sup>2</sup> instead of 40x320 km<sup>2</sup> for GOME), the noise on the individual GOME-2 BrO measurements was found to be significantly increased in comparison to GOME. Therefore, an alternative UV shifted fitting window of 336–351.5 nm that has already been used for SCIAMACHY measurements (so-called “SCIAMACHY” fitting-window) was introduced in the GDP 4.3, which significantly reduced the noise level compared to the “GOME” fitting window. In the GDP 4.5, improved BrO DOAS settings have been implemented with the objective to stabilize the fit as much as possible and to minimize interferences with other trace gases, especially formaldehyde (Theys et al., 2011). An important difference with respect to past settings relies in the choice of the fitting window which has been extended towards shorter wavelengths (332-359 nm) in order to cover five BrO absorption bands. The detailed DOAS settings for the GOME-2 BrO retrieval as used for the tropospheric bromine monoxide data record are listed below:

- The DOAS slant column fit is performed in a larger fitting window further extended towards shorter wavelengths to cover five BrO absorption bands (332-359 nm). In addition to a noise reduction, several unwanted artefacts could be minimized (viewing angle dependent slant columns, interference with formaldehyde absorptions over polluted areas, presence of cloud structures due to incomplete ring effect correction).
- The daily solar reference is used, biases between the slant column densities are considered by the equatorial correction sec. 2.2.
- A single BrO cross-section at 223K is included in the fit (Fleischmann et al., 2004).
- In addition, cross-sections of the interfering trace gases ozone at 223K and 243K (BDM (Daumont et al. 1992; Brion et al., 1993; Malicet et al., 1995)), formaldehyde at 298K (Meller and Moortgat, 2000), OCIO at 293K (Bogumil et al., 2003) and NO<sub>2</sub> at 220K (Vandaele et al., 2002) are included.
- During the wavelength calibration fit the DOAS analysis tool determines the optimal slit function for 14 sub windows between 316 and 385 nm. The trace gas cross-sections are convoluted with the optimised slit function.
- Compensation of the molecular ring effect is been realized by including two Ring reference spectra as additional fitting parameters calculated by the SCIATRAN model (Rozanov et al., 2001).
- To consider the strong ozone absorption in the extended fitting window below 336 nm, two additional fitting parameters are included in the DOAS analysis (Puķīte et al., 2010). Here, the O<sub>3</sub> slant columns as function of wavelength and optical depth are described by Taylor series. The Taylor coefficients provide two additional cross-sections for O<sub>3</sub> at 223K (original cross-section multiplied by wavelength and original cross-section squared).
- The broadband filtering polynomial is of 5<sup>th</sup> order (6 coefficients).
- To correct for intensity offset effects, that may be induced by residual stray-light or remaining level-1 calibration issues, a linear offset correction is used by including an inversed earth-shine spectrum as additional effective cross-section in the DOAS fit.
- Two additional polarization functions (Eta and Zeta from GOME-2 calibration key data) are included in the fit (EUMETSAT, 2011).

## 2.2 Equatorial offset correction

The instrumental degradation, strongly showing up during the advanced lifetime of GOME-2A, negatively influences DOAS fit residuals, the noise in the BrO columns (see Figure 1). Although a daily solar reference is used, the SCDs show a decreasing trend. Therefore, an equatorial offset correction is applied on a daily basis to the BrO data (Richter et al., 2002). This correction enables to correct – to some extent – for the effect of the instrumental degradation on the total BrO column data time series.

For this correction, averaged BrO slant columns in the tropical latitudinal band between  $\pm 5^\circ$  are calculated on a daily basis, assuming small equatorial BrO columns with no significant seasonal variations. The averaged slant columns are then subtracted from all slant columns and a constant equatorial slant column offset of  $7.5 \times 10^{13}$  molec/cm<sup>2</sup> is added.

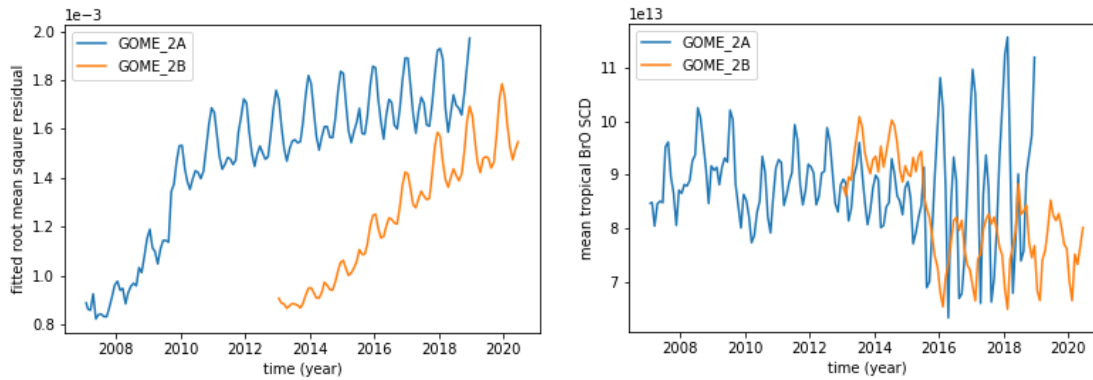


**Figure 1:** Long-term DOAS fitting residuals (left) and the (random) BrO slant column error (right) for the 332-359 nm BrO fitting window for GOME-2A and B. The monthly averaged residuals values and average slant column have been calculated for the equatorial region (10°S - 10°N). Due to the degradation of the GOME\_2A instrument, the data are not shown after end of 2018

## 2.3 AMF and VCD determination

The next step in the BrO column algorithm is the conversion of the slant column density  $S$  into the total vertical column  $V_{init}$ , using the AMF  $M$ :

$$V_{init} = \frac{S}{M} \quad (1)$$

The AMF depends on the vertical BrO profile and the so-called weighting function that contains the dependences on the GOME-2 viewing geometry, surface albedo, surface pressure and clouds. The radiative transfer calculations can be decoupled from the trace gas profile shape:

$$M = \frac{\sum m_l x_l}{\sum x_l} \quad (2)$$

where  $m_l$  is the box air mass factor for the individual layer  $l$  (independent of the BrO profile), and  $x_l$  the partial BrO column in layer  $l$ . The altitude-dependent air mass factors  $m_l$  are calculated with the LIDORT radiative transfer model for the window mid-point (345.5 nm), since BrO is an optically thin absorber in this wavelength region. The initial total VCD is computed under the assumption that the tropospheric BrO is negligible. Therefore, the air mass factor is based on stratospheric profiles only. This approach is roughly valid over large parts of the Earth, but in areas with significant tropospheric BrO, the total column densities are underestimated and need to be corrected, as

described in the next section. To incorporate seasonal and latitudinal variations in stratospheric BrO in the AMF calculations, a stratospheric BrO profile climatology is used (Theys et al., 2009). Detail of the stratospheric BrO profile can be found in next section. The climatology used for the surface albedo is derived from GOME-2 based directionally dependent Lambert-equivalent reflectivity (DLER) measurements at 340 and 354 nm, as described in Tilstra et al., 2017, and linear interpolated to 345.5nm.

For GOME-2 scenarios in the presence of clouds, the BrO air mass factor is determined using a Lambertian reflecting boundary cloud model (see Chapter 8 in GDP 4.8 ATBD (Valks et al., 2019)) and the independent pixel approximation (IPA):

$$M = (1 - w)M_{clear} + wM_{cloud}, \quad (3)$$

where  $M_{clear}$  is the air mass factor for a completely cloud free pixel,  $M_{cloud}$  the air mass factor for a completely cloudy pixel, and  $w$  the cloud radiance fraction.

## 2.4 Tropospheric BrO column

### 2.4.1 Stratospheric BrO correction

Firstly, the stratospheric BrO profiles are estimated using a new stratospheric BrO climatology (Theys et al., 2009) which is based on the output of the chemical transport model BASCOE. It can be written as

$$BrO = Br_y \times \frac{BrO}{Br_y}, \quad (4)$$

where  $Br_y$  is the inorganic bromine profile accounting for all inorganic bromine species (active bromine and bromine reservoirs). The impact of the stratospheric dynamics on the stratospheric BrO distribution is accounted for by means of  $Br_y$ /ozone correlations, while photochemical effects are determined by considering the stratospheric NO<sub>2</sub> columns as an indicator of BrO/ $Br_y$  ratio. The operational total ozone and stratospheric NO<sub>2</sub> columns products from the same GOME-2 measurement are directly used to calculate  $Br_y$  and BrO/ $Br_y$  as indicators of the dynamical and photochemical state of the atmosphere. Moreover, this approach allows saving computational resources as on-the-fly CTM simulations are not necessary. Secondly, the stratospheric BrO vertical columns are derived by integrating simulated stratospheric BrO profiles between the tropopause and the top-of-atmosphere. The tropopause is calculated using the potential vorticity (PV) from the meteorological data (mainly the wind and temperature fields) of European Center for Medium-Range Weather Forecasts (ECMWF). Finally, to ensure consistency with GOME-2 measurements a fine adjustment of the climatology is executed. The correction is based on the fact that stratospheric  $Br_y$  match closely the ozone variability. It consists in adjusting the slope of modelled BrO/O<sub>3</sub> VCD correction plot to the measured total BrO/O<sub>3</sub> VCD. In practice, the modelled and measured total BrO columns are selected for two mid-latitudinal bands (40-45° N and 40-45° S) to construct separate correction for the Northern and Southern Hemispheres (Theys et al., 2011).

## 2.5 Tropospheric Air Mass Factor and VCD computation

After the estimation of stratospheric BrO vertical column ( $V_s$ ), the tropospheric vertical column ( $V_t$ ) can be determined according to the following equation:

$$V_t = \frac{S - M_s V_s}{M_t}, \quad (5)$$

where  $S$  is the slant column density and  $V_s$  is the stratospheric columns derived using the method described above.  $M_s$  is the stratospheric air mass factor, used for the calculation of the total VCD,

as described in Sect. 1.3 of ATBD (Valks et al., 2019).  $M_t$  is a tropospheric air mass factor calculated with Eq. (2), using an a priori tropospheric BrO profile. Two different approaches are used depending on the surface albedo value because the vertical distribution of BrO in the troposphere is largely unknown. For high albedo situations (>50%), we used a tropospheric BrO concentration profile constant in the first 2 km above the Lambertian surface reflector. For low albedo situations, a Gaussian profile with a maximum at 6 km high and a full width half maximum of 3 km is used.

For many measurements over cloudy scenes, the cloud-top is well above the tropospheric BrO abundance in the boundary layer, and when the clouds are optical thick, the enhanced tropospheric BrO concentrations cannot be detected by GOME-2. To minimize the bias resulting from clouds, the analysis includes only the measurements with a cloud fraction < 50%. Independent of the cloud fraction we calculated an effective scene height, as cloud fraction weighted mean of cloud height and terrain height.

Surface covered by snow or ice are important for the retrieval of tropospheric BrO because the large concentrations of BrO in the polar boundary layer are generally observed over bright surface. Therefore daily sea ice concentrations from EUMETSAT's OSI-SAF project (Lavergne, 2019, <http://osisaf.met.no/p/ice/index.html#conc-cont-reproc-v2>) are included in a daily update of the in the albedo map combined with ECMWF-ERA-5 reanalysis snow cover and snow albedo data. If the snow or ice fraction of the 0.25° grid exceeds a threshold of 20% the respective data are flagged. The respective albedo is given by the weighted mean of the snow albedo and 0.05 for land, or 0.9 and 0.06 for ice and water respectively. OCRA is able to derive an effective cloud fraction for high albedo scenes, although underestimation of cloud fraction is expected for the snow/ice scenes (Lutz et al., 2016). To minimize this bias due to thick elevated clouds over snow/ice area the effective scene albedo and height were used if the surface albedo exceeds 0.5. When the effective scene was less than 700m above the surface, the difference was assumed to be negligible and the surface height used as lower boundary.

After the calculation of the tropospheric vertical column, a corrected total VCD  $V_c$  can be calculated via the relation:

$$V_c = V_s + V_t \quad (6)$$

An error estimate for the GOME-2 total and tropospheric BrO columns is given in Table 1.

**Table 1:** Estimation of error sources for the total and tropospheric BrO column.

Error source	Percent error	
	Total column	Tropospheric column
<b>BrO slant column</b>		
BrO absorption cross-sections	5-10	5-10
Instrument signal-to-noise	10-20	10-20
<b>Stratospheric BrO column</b>	n.a.	25
<b>BrO equatorial correction</b>	1e13/AMF	1e13/AMFtrop
<b>BrO Air Mass Factor</b>	5-20	20-50 (tropics-midlat/polar)
<b>BrO vertical column (accuracy)</b>	20-50	70-100

### 3. REFERENCES

- Bogumil, K., Orphal, J., Homann, T. Voigt, S., Spietz, P., Fleischmann, O. C., Vogel, A., Hartmann, M., Bovensmann, H., Frerik, J., and J.P. Burrows (2003), Measurements of Molecular Absorption Spectra with the SCIAMACHY Pre-Flight Model: Instrument Characterization and Reference Data for Atmospheric Remote-Sensing in the 230-2380 nm Region, *J.Photochem. Photobiol. A.*, 157, 167-184.
- Brion, J., Chakir, A., Daumont, D., Malicet, J., and Parisse, C.: High-resolution laboratory absorption cross section of O<sub>3</sub>. Temperature effect, *Chem. Phys. Lett.*, 213, 610–612, 1993.
- Daumont, Brion, J., Charbonnier, J., and Malicet, J.: Ozone UV spectroscopy I: Absorption crosssections at room temperature, *J. Atmos. Chem.*, 15, 145–155, 1992.
- EUMETSAT (2011), GOME-2 Products Guide, Ref.: EUM/OPS-EPS/MAN/07/0445, Issue: v3, Date: 17 Mar 2011.
- Fleischmann, O. C., Hartmann, M., Burrows, J. P. , Orphal, J., (2004), New ultraviolet absorption cross-sections of BrO at atmospheric temperatures measured by time-windowing Fourier transform spectroscopy, *J. photochem. photobiol., A Chem.*, 168, no1-2, 117-132.
- Heue, K.-P. et al., (Dec 2020) Product User Manual of GOME-2 tropospheric BrO product, SAF/AC/DLR/PUM/BrOTrop/01, Iss 1A.
- Lavergne, T., Sørensen, A. M., Kern, S., Tonboe, R., Notz, D., Aaboe, S., Bell, L., Dybkær, G., Eastwood, S., Gabarro, C., Heygster, G., Killie, M. A., Brandt Kreiner, M., Lavelle, J., Saldo, R., Sandven, S., and Pedersen, L. T. ( 2019): *Version 2 of the EUMETSAT OSI SAF and ESA CCI sea-ice concentration climate data records*, *The Cryosphere*, 13, 49-78, [doi:10.5194/tc-13-49-2019](https://doi.org/10.5194/tc-13-49-2019),
- Lutz, R., Loyola, D., Gimeno García, S., and Romahn, F.: OCRA radiometric cloud fractions for GOME-2 on MetOp-A/B, *Atmos. Meas. Tech.*, 9, 2357-2379, [doi:10.5194/amt-9-2357-2016](https://doi.org/10.5194/amt-9-2357-2016), 2016.
- Malicet, Daumont, D., Charbonnier, J., Parisse, C., Chakir, A., and Brion, J.: Ozone UV spectroscopy. II. Absorption cross-sections and temperature dependence, *J. Atmos. Chem*, 21, 263–273, 1995.
- Meller, R., and G. K. Moortgat (2000), Temperature dependence of the absorption cross sections of formaldehyde between 223 and 323 K in the wavelength range 225–375 nm, *J. Geophys. Res.*, 105(D6), 7089–7101, [doi:10.1029/1999JD901074](https://doi.org/10.1029/1999JD901074).
- Puķīte, J., S. Kühn, T. Deutschmann, U. Platt, and T. Wagner (2010), Extending differential optical absorption spectroscopy for limb measurements in the UV, *Atmos. Meas. Tech.*, 3, 631-653.
- Richter, A., and J. Burrows (2002), Tropospheric NO<sub>2</sub> from GOME measurements, *Adv. Space Res.*, 29, 1673-1683.
- Richter, A , F. Wittrock, M. Eisinger and J. P. Burrows (1998), GOME observations of tropospheric BrO in Northern Hemispheric spring and summer 1997, *Geophys. Res. Lett.*, No. 25, pp. 2683-2686.
- Rozanov, A., Rozanov, V., and Burrows, J. P. (2001), A numerical radiative transfer model for a spherical planetary atmosphere: Combined differential integral approach involving the Piccard iterative approximation, *J. Quant. Spectrosc. Radiat. Transfer*, 69, 491–512.
- Siddans, R., B.J. Kerridge, B.G. Latter, J. Smeets and G. Otter (2006), Analysis of GOME-2 Slit function measurements, Algorithm Theoretical Basis Document, EUM/CO/04/1298/RM.
- Siddans, R., Kerridge, B.J., Latter, B. G., Smeets, J., Otter, G. (2012): Analysis of GOME-2 Slit function Measurements Algorithm Theoretical Basis Document, Eumetsat Contract No. EUM/CO/04/1298/RM.
- Theys, N., Van Roozendael, M., Errera, Q., Hendrick, F., Daerden, F., Chabrillat, S., Dorf, M., Pfeilsticker, K., Rozanov, A., Lotz, W., Burrows, J. P., Lambert, J.-C., Goutail, F., Roscoe, H. K., and De Mazière, M. (2009): A global stratospheric bromine monoxide climatology based on the BASCOE chemical transport model, *Atmos. Chem. Phys.*, 9, 831–848, <http://www.atmos-chem-phys.net/9/831/2009/>.
- Theys, N., Van Roozendael, M., Hendrick, F., Yang, X., De Smedt, I., Richter, A., Begoin, M., Errera, Q., Johnston, P. V., Kreher, K., and De Mazière, M. (2011), Global observations of tropospheric BrO columns using GOME-2 satellite data, *Atmos. Chem. Phys.*, 11, 1791-1811.
- Tilstra, L.G., Tuinder, O.N.E., Wang, P., Stammes, P. (2017): Surface reflectivity climatologies from UV to NIR determined from Earth observations by GOME-2 and SCIAMACHY. *J. Geophys. Res. Atmos.*, 122, [doi:10.1002/2016JD025940](https://doi.org/10.1002/2016JD025940),
- Vandaele, A. C., C. Hermans, S. Fally, M. Carleer, R. Colin, M.-F. Merienne, A. Jenouvrier, and B. Coquart (2002), High-resolution Fourier transform measurement of the NO<sub>2</sub> visible and near-infrared absorption cross section: Temperature and pressure effects, *J. Geophys. Res.*, 107(D18), 4348, [doi:10.1029/2001JD000971](https://doi.org/10.1029/2001JD000971).
- Valks, P., et al., (2019) Algorithm Theoretical Basis Document for GOME-2 Total Column Products of Ozone, NO<sub>2</sub>, BrO, SO<sub>2</sub>, H<sub>2</sub>O, HCHO, OCIO and Cloud Properties (GDP 4.8/4.9), SAF/AC/DLR/ATBD/01, Iss. 3/B.

Valks, P. et al (Nov 2019) GOME-2 Level 2 Product User Manual (PUM) of Total Column Products of Ozone, NO<sub>2</sub>, BrO, HCHO, SO<sub>2</sub>, H<sub>2</sub>O, OCIO and Cloud Properties (GDP 4.8/4.9) SAF/AC/DLR/PUM/01, Iss. 3/B